1 Chemical Composition of Fresh and Aged Asphalt-Related Organic

Aerosols: From Ambient Observations to Laboratory Experiments

4 Peeyush Khare^{1,2,a}, Jo Machesky^{1,b}, Leah Williams³, Mackenzie Humes^{4,c}, Edward C. Fortner³,

- 5 Manjula Canagaratna³, Jordan E. Krechmer^{3,d}, Andrew T. Lambe³, Albert A. Presto⁴, Drew R.
- 6 Gentner^{1,5*}

7

2

- 8 Department of Chemical and Environmental Engineering, Yale University New Haven CT 06511 USA
- ²Laboratory of Atmospheric Chemistry, Paul Scherrer Institute, 5232 Villigen, Switzerland
- ³Aerodyne Research Inc. Billerica MA 01821 USA
- ⁴Center for Atmospheric Particle Studies, Carnegie Mellon University, Pittsburgh PA 15213 USA
- 12 ⁵School of the Environment, Yale University, New Haven CT 06511 USA
- ^aNow at: Institute of Climate and Energy Systems, ICE-3: Troposphere, Forschungszentrum Jülich GmbH, 52428
- 14 Jülich Germany
- 15 bNow at: United States Environmental Protection Agency, Durham NC 27709 USA
- 16 °Now at: California Air Resources Board, Riverside CA 92507 USA
- 17 dNow at: Bruker Scientific LLC., Billerica, MA 01821, USA
- 18
- 19 *Correspondence to: drew.gentner@yale.edu

20

21

Abstract

- 22 Asphalt-related emissions are an understudied source of reactive organic compounds with the
- potential to form organic aerosols (OA). Ambient aerosol mass spectrometry (AMS)
- 24 measurements of asphalt-related aerosols near a month-long road paving project showed
- 25 enhanced ambient OA concentrations with a mix of primary and secondary OA signatures. For
- comparison, gas-phase emissions from real-world road asphalt samples at application (e.g.,
- 27 140°C) and in-use (e.g., 60°C) temperatures were injected into an environmental chamber and an
- 28 oxidation flow reactor to simulate varying degrees of oxidative aging, while measuring their gas-
- and aerosol-phase oxidation products. Secondary OA formation was observed via both self-
- 30 nucleation and condensation with chemical properties dependent on asphalt temperature and
- 31 reaction conditions. The chemical composition of less-aged asphalt-related OA observed in
- 32 outdoor and laboratory measurements was similar to OA from other petrochemical-based sources
- and hydrocarbon-like OA source factors observed via AMS in previous urban studies. The
- 34 composition of aged OA varied with degree of oxidation, similar to oxidized OA factors
- 35 observed in ambient air. Taken together, these field and laboratory observations suggest that
- 36 contributions to urban OA during and after application may be challenging to deconvolve from
- 37 other traditional sources in ambient measurements.

- 39 Keywords: Road paving, intermediate- and semi-volatile organic compounds, volatile chemical
- 40 products, organic aerosol, time-of-flight aerosol mass spectrometry

Synopsis: Ambient observations and laboratory oxidation experiments show the chemical composition of asphalt-related organic aerosol production resulting from multiple formation processes with properties similar to that frequently observed in urban organic aerosols.

45

46

1. Introduction

- 47 Airborne fine-mode particulate matter (PM_{2.5}) is largely comprised of organic and inorganic
- 48 aerosols that play important roles in air quality and human health. Organic aerosol (OA) now
- represents a dominant fraction of U.S. PM_{2.5}¹ and includes both primary organic aerosol (POA)
- that is directly emitted, and secondary organic aerosol (SOA) that forms via atmospheric
- oxidation of reactive gas-phase precursors.^{2,3} These precursors include volatile (VOCs),
- 52 intermediate volatility (IVOCs) and semi-volatile organic compounds (SVOCs) that are emitted
- from a diverse mix of anthropogenic and biogenic sources with varying and uncertain
- 54 contributions to urban SOA.^{4–10}
- Recent estimates suggest that SOA production from anthropogenic emissions of VOCs-SVOCs
- from non-combustion-related sources (e.g., volatile chemical products) now exceed annual SOA
- 57 contributions from on-road gasoline and diesel vehicles in developed cities. 5,11–13 Asphalt is one
- 58 urban source of I/SVOCs, which are important SOA precursors, with widespread urban use and
- emissions that can occur throughout its material lifecycle. 5,14–18 Yet, its emissions can vary
- 60 considerably depending on material properties, application methods, usage, age, and
- 61 geographically-varying environmental factors (e.g., summertime surface temperatures). 5,19
- 62 Several prior studies have estimated volatile content in asphalt via mass spectrometry and
- 63 gravimetric techniques, and emissions of methane, carbon monoxide and other bulk VOCs,
- polycyclic aromatic hydrocarbons (PAHs), and unspeciated lower volatility compounds (e.g.,
- 65 SVOCs) have also been shown. 11,20-27 Furthermore, the impact of asphalt-related emissions on
- air quality has been investigated in ambient, laboratory and modeling studies. 14,28–30 Notable
- examples include recent U.S. nationwide PM_{2.5} modeling effort with updated source profiles
- 68 including I/SVOCs, ¹⁴ long-term emissions estimations for samples collected in France and the
- 69 U.S., ^{19,29,30} and molecular-level investigations of asphalt/asphaltene oxidation from solar
- exposure. 26,31 Some occupational exposure studies have also investigated short-term, near-source
- exposure of construction workers to ambient hot-mix paving emissions with focus on bulk
- 72 particulate matter concentrations and select PAHs. 32-34 All these varied measurements identify
- asphalt as a non-negligible source of reactive organic compounds. The chemical composition and
- 74 properties of OA resulting from asphalt-related emissions is not well established either from real-
- world ambient observations³⁵ or laboratory studies, especially in comparison to other typical
- 76 urban sources (e.g. gasoline and diesel exhaust).

- 78 Laboratory oxidation chambers and flow reactors (OFRs) simulate atmospheric chemical
- 79 processes with typical atmospheric oxidants (i.e., OH, NO₃, O₃) to simulate SOA formation from
- single reactive precursors or mixtures.^{36–41} While larger Teflon-lined chambers generally
- simulate short-term aging (6-10 hours) with atmospherically relevant oxidant concentrations,
- OFRs can perform multi-day aging in minutes with high levels of oxidant exposure. Both have
- been used widely with complex precursors from other sources that vary in composition and
- magnitude with time (e.g. evaporative emissions from crude oil, ambient air, vehicle exhaust). 42–
- 85 48
- 86 The overall objective of this study was to use a combination of ambient and laboratory
- 87 observations to examine the chemical composition of asphalt-related OA with varying degrees of
- atmospheric oxidation. Ambient measurements in the vicinity of a 1-month long road paving
- 89 event in Billerica, MA, were compared with laboratory experiments simulating short- and
- 90 longer-term atmospheric aging to examine the chemical composition of the OA formed from
- 91 asphalt-related emissions at application and elevated summertime in-use temperatures. Lastly,
- 92 we compared the chemical composition of our ambient and lab-generated asphalt-related OA to
- 93 the OA produced from diverse sources in prior laboratory experiments, and also with well-
- 94 established ambient OA factors from previous studies in urban areas.

96

2. Materials and Methods

- 97 Ambient aerosol chemical composition measurements
- 98 Measurements of ambient sub-micron particle chemical composition and size were performed at
- 99 Aerodyne Research, Inc. using a high-resolution time-of-flight aerosol mass spectrometer (HR-
- ToF-AMS, Aerodyne, SN 215-122). The measurements occurred during 1–26 August 2014 that
- coincided with nearby asphalt-paving activities and also during 27 August 20 September 2020
- that were under routine conditions without paving. Ambient air was sampled at 3 L min⁻¹ through
- a 2.5 μm cut cyclone on an elevated outdoor platform outside of the Aerodyne Research Facility
- of 45 Manning Rd., Billerica, MA (42.53, -71.27, 60 m a.s.l.), located ~200 m east of a major
- freeway (US Route 3, see Figure S1).
- The AMS sampled particles through a 100 µm critical orifice and a standard aerodynamic lens
- that transmits particles with vacuum aerodynamic diameters in approximately 70 nm 700 nm
- size range (d_{va}, Liu et al., 2007), ⁴⁹ forming a focused particle beam that is transmitted into the
- detection region. Here, the non-refractory species are flash vaporized upon impact with a hot
- surface (600°C). The particle vapor was ionized using electron impact ionization (70 eV) and
- detected by the time-of-flight mass spectrometer (DeCarlo et al., 2006). ⁵⁰ Particle size (particle
- time of flight, pToF) data was determined from the particle flight time in the vacuum chamber
- after passing through a chopper.

- Providing baseline measurements over a longer time period, additional particle chemical
- composition measurements were acquired for multiple days at a time from June 2013 to
- December 2014 using various aerosol chemical speciation monitors (ACSMs). The ACSM
- operates on the same principle as the AMS but without any particle size differentiation below its
- PM₁ size cut. These instruments included either a quadrupole mass spectrometer or a unit mass
- resolution time-of-flight mass spectrometer. All instruments had a standard PM₁ lens and
- sampled from the roof without a cyclone.
- The AMS and ACSM instruments were calibrated for ionization efficiency of nitrate and relative
- ionization efficiency of ammonium and sulfate using size-selected single component particles of
- ammonium nitrate or ammonium sulfate following Budisulistiorini et al.⁵¹ HR-ToF-AMS data
- were analyzed with Squirrel (1.63I) and Pika (1.23I) analysis software running in Igor 7
- 125 (WaveMetrics, Inc.). ACSM data was analyzed with Tofware (3.2.40211B2) or ACSM Local
- 126 (v1.6.1.1). The collection efficiency (CE) was set to 0.5 for all data.⁵² Positive matrix
- factorization (PMF), a typical statistical method for analyzing OA contributions to PM, was used
- to determine source factor contributions from common AMS PMF factors (e.g., HOA, BBOA,
- LO-OOA, MO-OOA). PMF analysis of the HR-ToF-AMS data was performed in PMF
- Evaluation Tool (PET 3.06, Ulbrich et al., 2009). Mass spectra for other sources or urban areas
- for comparison were from the references herein (Tables S2-S3).
- 132 Oxidation chamber experiments
- For short-term (i.e., less-aged) experiments, gas-phase emissions were sampled off of a large
- piece (99.3 grams) of recently-paved (i.e. collected ~28 hours after application) asphalt from an
- arterial roadway (grade unknown) that was heated to 140°C with no UV exposure to the sample.
- The fumes were injected via a Teflon tube into a 10 m³ Teflon chamber with 1 slpm clean
- airflow to evaluate the production of primary OA without photooxidation. Subsequently, the UV
- lights (peak $\lambda = 368$ nm) were turned on to initiate secondary production under high NO_x (4.5
- ppm) conditions via HONO photolysis. HONO was produced from reacting 25 mL of dilute
- sodium nitrite solution (10 g/L, > 99% Sigma-Aldrich, St. Louis, MO) with sulfuric acid
- 141 (95/98% Sigma-Aldrich, St. Louis, MO). It was subsequently bubbled into the chamber for
- photolysis. The chamber was maintained at 25 °C under relatively dry conditions (<10% relative
- humidity) and an OH concentration of $\sim 1 \times 10^{-7}$ molecules cm⁻³ during the first hour of
- oxidation. Deuterated butanol (d9-butanol; 90% Cambridge Isotope Laboratories) was also
- injected into the chamber via a heated septum injector as an OH tracer ($k_{OH} = (3.4 \pm 0.88) \times 10^{-12}$
- cm³ molecule⁻¹ s⁻¹), which was measured using a quadrupole proton transfer reaction mass
- spectrometer (PTR-MS, Ionicon Analytik, Innsbruck, Austria). The particle-phase effluent from
- the chamber was measured using an HR-ToF-AMS.
- 149 Oxidation flow reactor experiments
- Daytime and nighttime oxidative studies of gas-phase asphalt emissions simulating a range of
- photochemical ages were conducted using a Potential Aerosol Mass OFR; Aerodyne Research,

```
Inc.), which is a horizontal 13 L cylindrical aluminum chamber (46 cm long × 22 cm ID)
152
            operated in continuous flow mode, with 10 L min<sup>-1</sup> flow through the reactor. The calculated
153
            mean residence time in the OFR was approximately 80 s. Across all OFR experiments, the input
154
            relative humidity (RH) was controlled with a Nafion membrane and ranged 30-41% at OFR
155
            temperatures ranging 26-28°C. For OH-OFR studies, OH was generated from the combined
156
            photolysis of O_2 and H_2O at \lambda = 185 nm plus photolysis of O_3 at \lambda = 254 nm using two low-
157
            pressure germicidal mercury lamps. In a subset of experiments, NO<sub>x</sub> was also generated from
158
            O(<sup>1</sup>D) + N<sub>2</sub>O reactions following addition of 260-730 cm<sup>3</sup> min<sup>-1</sup> of N<sub>2</sub>O to the OFR carrier gas
159
            flow. 54,55 For NO<sub>3</sub>-OFR studies simulating nighttime chemistry, N<sub>2</sub>O<sub>5</sub> vapor was continuously
160
            generated in a laminar flow reactor (LFR) from the reactions NO_2 + O_3 \rightarrow NO_3 + O_2 and NO_3 + O_3 + O_
161
            NO_2 \rightarrow N_2O_5. The N_2O_5 was then continuously injected into the dark OFR, where co-injected
162
            asphalt-related emissions were exposed to NO<sub>3</sub> generated from room-temperature thermal
163
            decomposition of the N<sub>2</sub>O<sub>5</sub>.<sup>58</sup>
164
            Prior to experiments, PG 64-22 grade road asphalt samples were collected from a New Haven,
165
            CT paving site and stored in a sealed container. For each experiment, new specimens of this
166
            asphalt were heated to surface temperatures achieved during summer daytime in-use and
167
            application (60° - 140°C) in a custom-made portable heated chamber described in detail
168
            elsewhere.<sup>5</sup> The gas-phase emissions were continuously injected into the OFR via a 10 cm
169
            heated stainless steel transmission line at a flow rate of 1 L min<sup>-1</sup> with an additional 9 L min<sup>-1</sup> of
170
            clean dilution air. The estimated total initial I/SVOC mixing ratios (also including minor
171
            contributions of C<sub>10</sub> – C<sub>12</sub> VOCs) introduced to the OFR were 19 ppbv (60°C) and 112 ppbv
172
            (140°C). To calculate the corresponding total external OH and NO<sub>3</sub> reactivities (OHR<sub>ext</sub>,
173
            NO<sub>3</sub>R<sub>ext</sub>) of the emissions, we assumed mean I/SVOC + OH and I/SVOC + NO<sub>3</sub> reaction rate
174
            coefficients of 4×10<sup>-11</sup> (Robinson et al., 2007) and 1×10<sup>-13</sup> cm<sup>3</sup> molecule<sup>-1</sup> s<sup>-1</sup> (applying the
175
            acenaphthene-NO<sub>3</sub> rate coefficient<sup>53</sup> of 4.6×10<sup>-13</sup> cm<sup>3</sup> molecules<sup>-1</sup> s<sup>-1</sup> to the ~ 25% aromatic
176
            fraction of asphalt I/SVOCs<sup>5</sup> and assuming the remaining I/SVOCs were unreactive towards
177
            NO<sub>3</sub>). The calculated OH exposures were approximately (3.0 - 6.9) \times 10^{10} molecules cm<sup>-3</sup> s
178
            (OHR_{ext} = 110 \text{ s}^{-1}) and (1.3 - 2.6) \times 10^{11} molecules cm<sup>-3</sup> s (OHR_{ext} = 19 \text{ s}^{-1}) using an estimation
179
            equation derived by Rowe et al. (2020), with an estimated uncertainty of \pm 50\%. These OH
180
            exposures correspond to 0.2 - 0.5 and 1 - 2 equivalent days of atmospheric exposure to [OH] =
181
            1.5×10<sup>6</sup> molecules cm<sup>-3</sup> for 140°C and 60°C experiments, respectively.<sup>57</sup> The calculated NO<sub>3</sub>
182
            exposures in the OFR were approximately (4-8)\times10^{13} molecules cm<sup>-3</sup> s (NO_3R_{ext} = 0.27-0.05 \text{ s}^{-1})
183
            following Lambe et al. <sup>56</sup> These NO<sub>3</sub> exposures correspond to ~1 day of equivalent atmospheric
184
            exposure to [NO_3] = 5.0 \times 10^8 molecules cm<sup>-3</sup> s (Atkinson et al., 1991). In all experiments, the
185
            particle-phase effluent from the OFR was analyzed using an Aerodyne ToF-AMS, while the gas-
186
            phase effluent was measured using a Vocus proton transfer reaction (PTR)-ToF mass
187
            spectrometer in a subset of experiments (TOFWERK AG).
188
```

3. Results and Discussion

189

3.1 Ambient observations of asphalt-related organic aerosol

191

AMS-based field measurements were performed at the Aerodyne Research site in Billerica, MA 192 in August 2014. These measurements coincided with a number of paving projects in areas 193 surrounding Aerodyne including documented projects on I-95 (MA DOT Project 606170) as well 194 as other paving activities nearby (e.g. US Route 3) (Figure S1). Aerodyne Research is 195 approximately 7 km north/northwest of I-95. During the day, the wind was typically from the 196 south and the average windspeed was 3-5 km hr⁻¹ meaning that paving emissions would arrive 197 at Aerodyne in about 1-2 hours, or less in the case of more nearby paving (Figure S2). At night, 198 windspeeds were very low, typically below 0.5 km hr⁻¹ and wind direction was variable. The 199 observations provided the opportunity to investigate the chemical composition of primary and 200 secondary asphalt-related OA beyond the immediate vicinity of a freshly paved surface. Figure 1 201 shows a large increase in monthly average PM₁-sized OA concentrations (monthly average: 202 18±13 μg m⁻³) at the Aerodyne site in August, 2014. This enhancement is observed not only 203 when compared to the rest of 2013-2014 (avg: 3.3±1.9 μg m⁻³, excluding August), but also to 204 August/September 2020 (monthly average: 3±2 μg m⁻³), the closest year for which we had a late 205 summer month of AMS data sampled from the Aerodyne roof. The 2020 average at Aerodyne is 206 similar to regional OA in 2022 in other urban areas in the northeast US (3.1±0.6 μg m⁻³; Figure 207 1). 59-61 Figure 2 shows the AMS measurements during August 2014 in more detail. In 208 comparison to before and after the measurement intensive period, the OA concentrations were 209 elevated throughout the month (Figures 1-2a). During August 1 - 11, OA concentrations ranged 210 between 8.5 and 66 µg m⁻³ (2-min averages) (Figure 2a) followed by a decrease over next 3 days 211 due to minor precipitation events (i.e., $0.8-17 \mu g m^{-3}$). Thereafter, OA was generally elevated 212 again during August 16 - 25, ranging $4 - 39 \mu g m^{-3}$. The highest loadings were observed on 213 August 26 reaching a 24-hr average of $90\pm79~\mu g~m^{-3}$ with a range of $27-516~\mu g~m^{-3}$ at 2-min 214 resolution. For comparison, OA at the same location averaged 3±2 µg m⁻³ during August – 215 September 2020, which was similar to the 2013-14 measurements outside of the paving period. 216

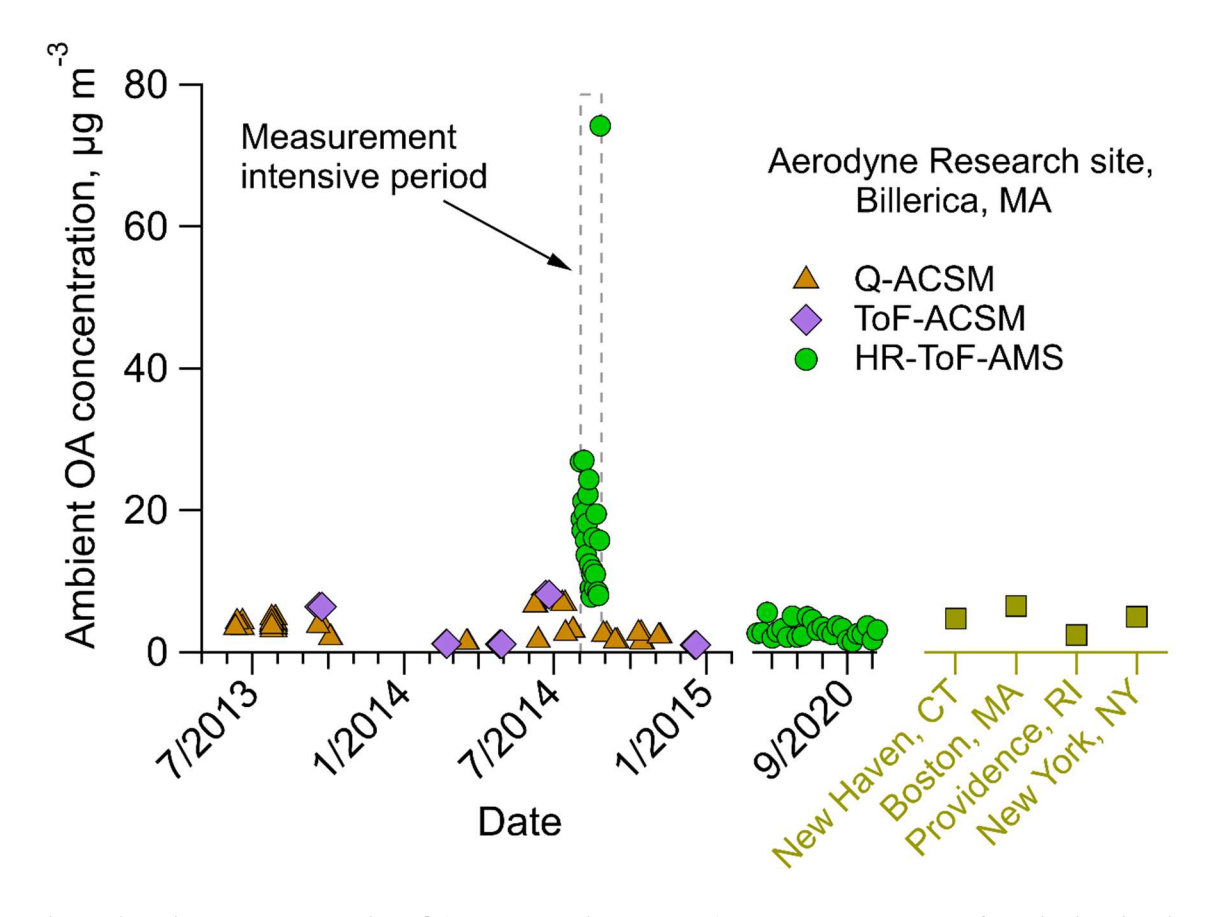


Figure 1. Daily averaged ambient OA concentrations at the Aerodyne Research rooftop site in Billerica, MA using 3 variants of aerosol mass spectrometers, with average ambient OA concentrations for nearby urban areas (brown) for comparison, including New Haven (2014)^{59,62}, Boston (2008)⁶⁰, Providence (2022)⁵⁹ and New York City (2014).^{61,62} The ambient OA concentrations for New Haven and Providence were estimated using the annually averaged measurements of organic carbon via EPA's Chemical Speciation Network⁵⁹ using an organic mass-to-organic carbon (OM:OC) ratio of 2 based on prior studies.^{63,64} The calculated OA concentrations were consistent with previous airborne measurements of ambient organic aerosol in these regions.⁶¹

The persistent OA enhancements in August 2014 suggest prolonged emissions during the nearby road paving project. This was not a region-wide enhancement as regional daily PM_{2.5} measured at the MA Department of Environmental Protection von Hillern station (18 miles away) was similar across 2014 – 2020 (Figure S3b-c). The local OA was enhanced by a factor of 5.1 when normalized to regional PM_{2.5} (i.e., ratio of medians in Figure 2a inset) highlighting the proximity of the source. Despite the lingering effects of the pandemic-related shutdown, small changes in traffic volume in 2020 were not enough to explain the large difference in OA in August 2014 relative to 2020 (Figure S3a). Furthermore, the size distribution of measured OA was different between the two periods. The ion signal at m/z 57 (characteristic fragment for hydrocarbons) peaked at ~550 nm in August 2014, shifted from more typical observations in September 2020 (~375 nm) and with 8 times higher mass loading (Figure S4).

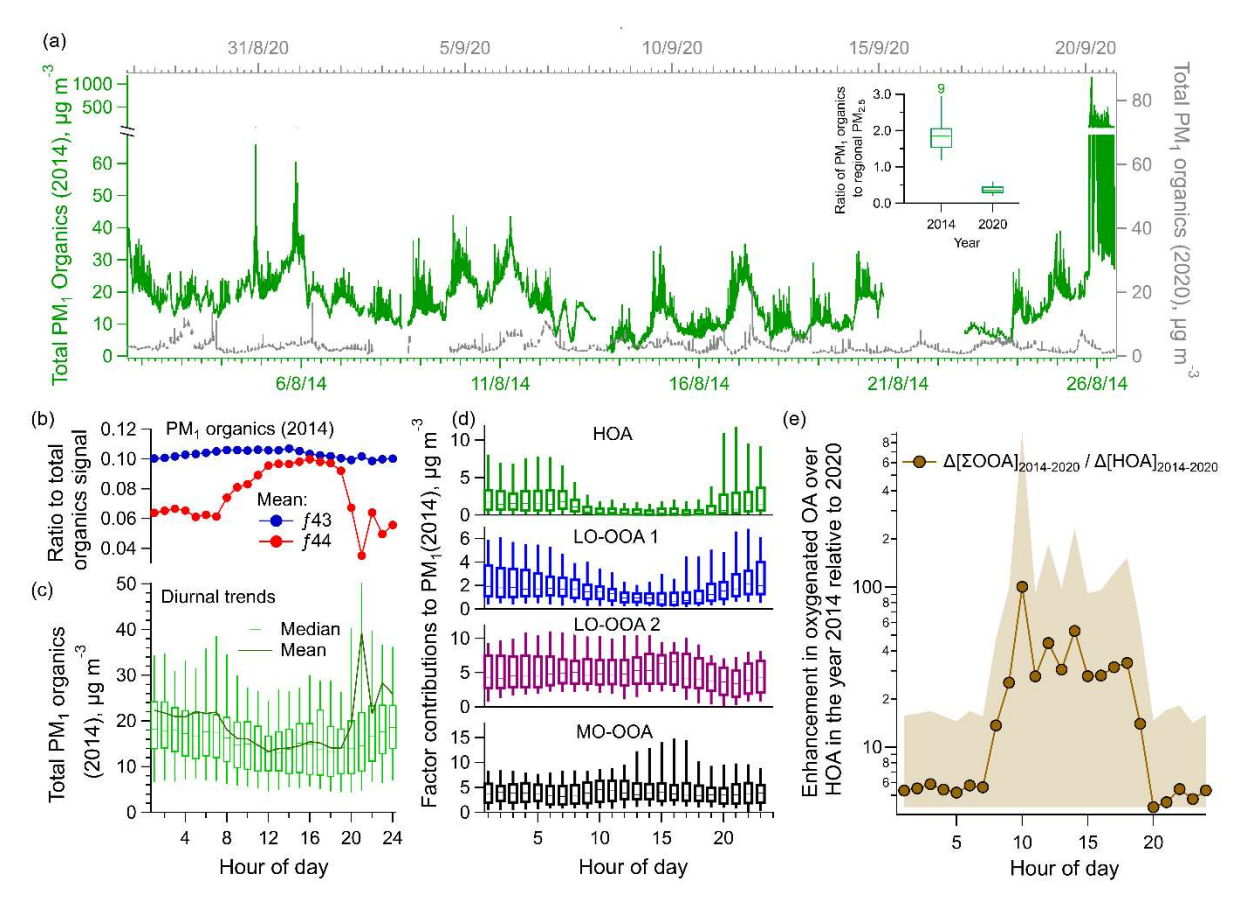


Figure 2. (a) OA concentrations (PM₁) measured with an AMS during August 2014 and September 2020 at the Aerodyne Research rooftop site, with (inset) a comparison of local OA to regional PM_{2.5} ratios for 2014 and 2020 showing 0th, 25th, 50th, 75th, and 100th percentiles, despite similar regional PM_{2.5} concentrations (2014: 9.2 μg m⁻³; 2020: 8.0 μg m⁻³; Figure S3). Diurnal trends in August 2014 for (b) f₄₃ and f₄₄ ion fragments of the AMS spectra with (c) mean and median concentrations of total measured OA and (d) source factor contributions to OA in August 2014. (e) Diurnal enhancement in total oxygenated organic aerosol over HOA (ΣΟΟΑ/HOA) in August 2014 relative to September 2020. All data in EST.

The five OA factors determined via PMF (section S1, figures S5-7) for August 2014 and three for September 2020 (figures S8-9) showed different diurnal trends between the two periods that would arise from variations in contributing sources. For example, HOA in August 2014, during the road paving operations, was typically high overnight, from evening to early morning (8 PM − 6 AM) (Figure 2d), as opposed to morning (6 AM − noon) enhancement in September 2020 typical of commute-related maxima due to vehicular emissions (Figures S7-9). Furthermore, the maximum nighttime HOA averages were 2 − 6.5 times higher in August 2014 than in September 2020. Daytime HOA was similar across the 2 periods, consistent with major roadway asphalt application activities often occurring at night. Yet, the amount of OOA during daylight hours was significantly enhanced in August 2014 relative to September 2020 (Figure 2b, e, S10), suggesting SOA production leading to average ∑OOA/HOA ratios exceeding 20 μg/μg.

- More broadly, the mean diurnal OA concentrations in August 2014 showed meteorologically-
- influenced trends (Figure 2c). The mean concentration dropped from 22 μg m⁻³ at 7 AM to a
- minima of $13 \mu g \text{ m}^{-3}$ at noon, increasing some throughout the remainder of the day before
- returning to elevated levels with nightfall (i.e., $22 40 \mu g \text{ m}^{-3}$). The contribution of hydrocarbon-
- 261 like organic aerosol (HOA) to total OA was significantly reduced between 8 AM 6 PM, while
- the three factors contributing to total oxygenated organic aerosol (OOA) showed trends distinct
- 263 from each other.
- The less oxidized OOA factor (LO-OOA1) was characterized by a major C₂H₃O⁺ fragment on
- 265 m/z 43 in addition to $C_3H_7^+$, and an O:C ratio of 0.25. LO-OOA1 was likely affected by
- boundary layer dilution in the afternoon (Figure 2d: LO-OOA1) with median diurnal
- 267 concentrations dropping from nighttime averages of 1.4 μ g m⁻³ to 0.6 μ g m⁻³ in the afternoon.
- 268 These diurnal patterns varied from LO-OOA2, which remained elevated throughout the day, but
- dropped in the late evening, suggesting differences in OOA formation pathways that may be
- associated with emissions pathways or chemical processes across the gas- and particle-phase, or
- possibly variations in direct HOA emissions with the onset of paving activity. LO-OOA2 was
- more oxidized than LO-OOA1 with a higher O:C ratio of 0.5 and greater CO₂⁺ signal on m/z 44.
- 273 More oxidized OOA (MO-OOA) was the most aged with an O:C ratio of 0.8. The median
- 274 diurnal concentration of MO-OOA was relatively similar across both the night and day, despite
- enhanced daytime dilution possibly due to enhanced OOA production and aging from
- atmospheric oxidation of precursor emissions, or additional production pathways.
- On average, the total OOA including all observed OOA factors was a factor of 8 higher in
- August 2014 compared to September 2020 (Figures 2, S6, S8), with average contributions of
- 279 11.5±5.7 μg m⁻³ vs. 1.5±0.8 μg m⁻³, respectively. For comparison, average HOA contributions
- were $1.6\pm2.5~\mu g~m^{-3}$ vs. $0.5\pm0.4~\mu g~m^{-3}$ during the respective intensive periods. Σ OOA/HOA
- ratios varied dynamically (Figure 2a,e), likely with on-site activities (e.g., application) and
- environmental conditions (e.g., solar irradiance), ranging 0.8 267.4 (at hourly resolution) with
- an overall average of 24.2±34.0 μg μg⁻¹ during the 2014 measurement intensive period,
- corresponding to ~88% of OA during the paving period occurring as OOA rather than HOA on
- average. For comparison, subtracting the 2020 average HOA and OOA to consider only elevated
- levels in 2014, this value varied over the course of the day and was ~90% OOA on average
- 287 $(\Delta [\Sigma OOA]_{2014-2020}/\Delta [HOA]_{2014-2020} = 9.2\pm14.7 \,\mu g \,\mu g^{-1})$ over the 1-month measurement period,
- similar to previous work, which reported that oxygenated OA formed post-application can
- exceed primary OA formed during application by a factor of $9 10^{30}$
- Overall, ambient observations showed substantially enhanced OA concentrations in August 2014
- 291 when road paving occurred nearby, though this project is not assumed to be representative of all
- 292 projects as the OA contributions from paving activities are expected to vary with asphalt
- 293 feedstocks (e.g., composition), material properties (e.g., modifier additions), application methods
- 294 (hot vs. warm mix), environmental conditions, and other site specifics (e.g., project size,
- 295 pavement thickness). The authors are also not aware of the exact asphalt grade or any added

- modifiers. We also note that while our analysis suggests a major role of asphalt-paving sources
- in the elevated ambient OA levels, other contributing sources during the observations in 2014
- and 2020 may also exist, and gasoline- and diesel-powered construction equipment used during
- paving likely also contributed to both HOA and OOA-precursor emissions in August 2014.
- However, it was not possible to isolate their impact via the measurements in this study.

302

3.2 Laboratory investigation of asphalt-related organic aerosol

- Field observations of OA from paving activities emphasized the need for laboratory chamber
- and OFR experiments for the purpose of comparing the resulting OA spectra to ambient
- measurements. In these tests, gas-phase precursor emissions from road asphalt at application
- 306 (140°C) and summertime daytime surface (60°C) temperatures were aged for a few hours and up
- to 1-2 equivalent days simulating urban oxidation conditions (Table S1). The results showed
- 308 that asphalt-related OA can range from hydrocarbon-like to highly-aged organic aerosols
- depending on differences in asphalt temperature and oxidation conditions. These results are
- 310 discussed in detail in the following subsections.
- 311 Chamber OA from high-temperature paving-related emissions
- 312 Short-term daytime aging was simulated in CMU's oxidation chamber to study the chemistry of
- emissions immediately following high-temperature asphalt application. Gas-phase precursors
- emitted at 140°C were injected into a seedless, oxidant-free (hereon: "dark") chamber, then the
- 315 lights were turned on after 3 hours to initiate photo-oxidation. We observed that injected
- 316 precursors rapidly formed unaged hydrocarbon-like OA within minutes under dark conditions
- 317 (Figure 3, S11). This dark chamber OA (HOA_{DC}) had mass spectra similar to a previous ambient
- AMS measurements (cosine similarity: $12^{\circ} 16^{\circ}$) made directly downwind of road paving, ³⁵
- 319 suggesting representative experimental conditions (Figure S12).
- The ambient HOA factor observed during August 2014 road paving in Billerica (HOA_{BL14}) was
- very similar to the HOA_{DC} from the chamber study (cosine similarity: 15°). Both HOA_{DC} and
- HOA_{BL14} were relatively unaged OA with comparable O:C ratios (0.03 vs. 0.05) that were much
- lower than 0.2 in HOA from September 2020 (HOA_{BL20}). The AMS spectra of HOA_{DC} was
- dominated by fragments with ion formula $C_nH_{2n+1}^+$ (e.g. m/z 29, 43, 57 and 71) that represented
- acyclic alkanes. Other major fragments included $C_nH_{2n-1}^+$ (e.g. m/z 27, 41, 55, 69 and 83) and
- $C_nH_{2n-3}^+$ (e.g. m/z 67, 79, 81, 95 and 109) that are both typically cycloalkanes, 65 and aromatic
- fragments (e.g. m/z 77, 91, 105 and 119). The dominance of non-aromatic fragments was
- 328 consistent with previously reported composition of asphalt-related precursor emissions at
- 329 140°C,⁵ and the aromatic fraction would also be somewhat susceptible to ring-opening during
- oxidation. 66,67 The contributions from functionalized fragments (C_xH_vO₁) to the HOA_{DC} spectra
- were expectedly minor under dark chamber conditions and were likely primary emissions
- 332 (Figure S11).

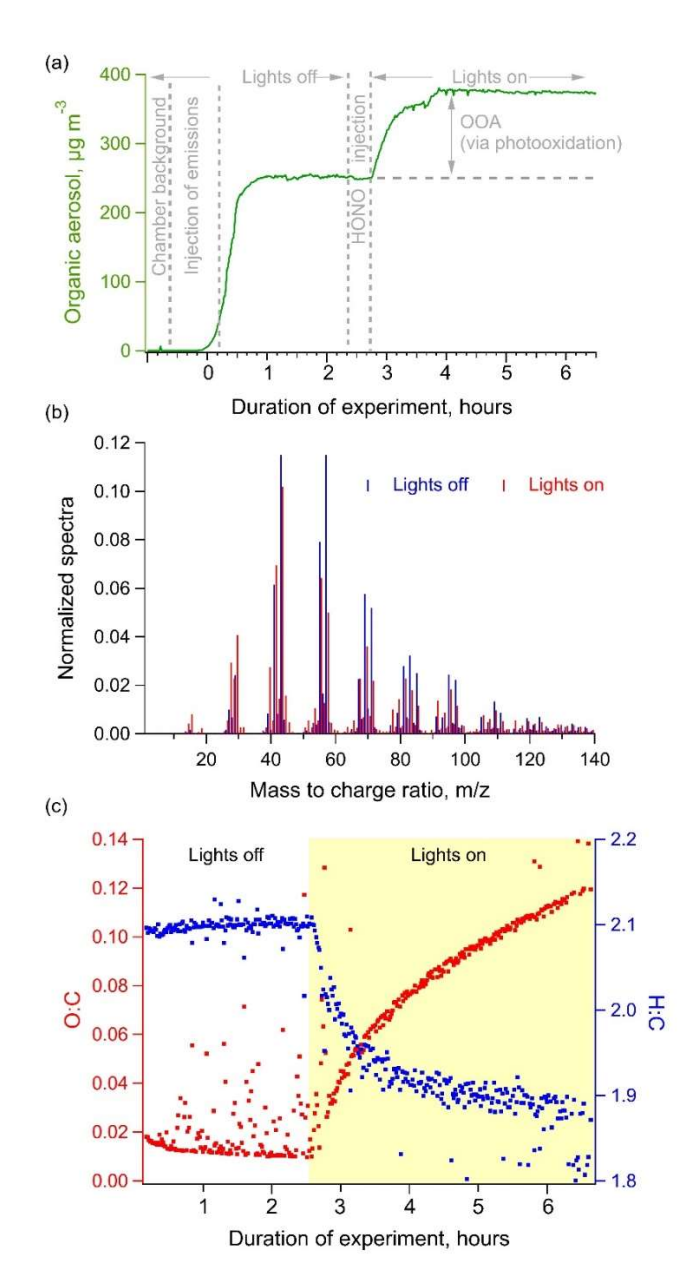


Figure 3. Asphalt-related OA formed in short-term chamber experiments from emissions at application temperatures. (a) OA concentrations measured via AMS (dia $\leq 1~\mu m$; wall-loss corrected) across the duration of the experiment. (b) AMS spectra of OA produced under dark conditions and following photo-oxidation with chamber lights on. (c) Bulk O:C and H:C ratios for organic aerosol before and during photo-oxidation.

After 2.4 hours, HONO was injected into the chamber and UV lights were turned on to simulate daytime conditions. This led to a 50% increase in OA concentrations after the equivalent of 6 hours of atmospheric aging, indicating SOA formation during which the bulk O:C ratio increased from 0.03 to 0.1 and the H:C decreased from 2.1 to 1.9 (Figure 3c). Via a modeling analysis, a similar change in ambient asphalt-related OA concentration was attributed to photochemistry by Seltzer et al. ¹⁴ By comparison, the enhancement in the year 2014 relative to 2020 ($\Delta\Sigma$ OOA/ Δ HOA) averaging 9.2±14.7 μ g μ g⁻¹ in ambient observations (Figure 2e) with greater overall O:C ratios indicates that over longer timescales following application, the majority of asphalt-related

- OA production will exhibit itself as oxygenated SOA, with variations with time of day, season,
- source proximity, and degree of photochemical aging. While Figure 3a has been corrected for
- particle losses to the chamber walls, the SOA production in this photooxidation experiment is a
- lower bound due to well-known losses of reactive I/SVOCs^{68,69} to the walls of the reaction
- 350 chamber during the 2.5 hr dark period.
- 351 The photo-oxidized chamber OA (OA_{LC}) showed comparable mass spectra to ambient LO-
- OOA1 from August 2014 (cosine similarity: 17°) with a similar H:C ratio (OA_{LC}: 1.9; LO-
- OOA1: 1.8). Yet, OA_{LC} was slightly less oxygenated than the ambient LO-OOA1 (O:C 0.1 vs
- 354 0.25) with oxygenated fragments constituting 21% of OA_{LC} (Figure S13) and ~35% of LO-
- OOA1. This broadly suggested that LO-OOA1 observed in the ambient measurements was
- inclusive of a combination of less-aged gas- or particle-phase asphalt-related emissions
- following paving, though some contributions from other combustion-based sources (e.g. diesel
- vehicles) is also possible.
- Photochemical aging also introduced differences between HOA_{DC} and OA_{LC} spectra. OA_{LC}
- constituted of more cyclic species (f_{55} : $f_{57} = 1.3$) than HOA_{DC} (0.7), which may be the result of
- 361 the oxidation and partitioning of gas-phase organic precursors and/or the aging of particle-phase
- species. The spectra of both OA types had similar relative contributions from large (> 150 m/z)
- and smaller hydrocarbon fragments (e.g. m/z 41, 43, 55), but OA_{LC} expectedly had more
- oxygenated fragments (e.g. m/z 28, 31, 44-46, 51), which is reflective of contributions from both
- unaged or less-aged hydrocarbons and condensed secondary oxygenated species.
- 366 *OA from longer-term simulated aging experiments*
- Gas-phase precursors emitted at both 140°C and 60°C were aged for longer effective durations
- (0.2-2) equivalent days) in an OFR. The extent of aging varied across experiments depending on
- the type of emissions and reactor conditions. The OA produced from emissions at 140°C in
- unseeded tests (OFR-OA_{US140}) was less aged (0.2 0.5 equivalent day) and resembled HOA. The
- mass spectrum of OFR-OA_{US140} was dominated by hydrocarbon fragments with an O:C ratio of
- 372 0.05, comparable to 0.03 for HOA_{DC}. Yet, 12% of f_{43} in its mass spectra was constituted by
- 373 C₂H₃O⁺, which was entirely C₃H₇⁺ in HOA_{DC}. Moderately-aged OA from a seeded experiment
- with the same emissions (OFR-OA_{S140}) had an O:C ratio of 0.18, yet hydrocarbon fragments still
- 375 dominated the mass spectrum.
- We also found that daytime (OH) vs. nighttime (NO₃) unseeded oxidation of emissions at 140°C
- produced OA with comparable mass spectra (Figure S14) and bulk properties (H:C 1.8; O:C –
- 378 0.05 vs. 0.09). This was somewhat unexpected because NO₃ is a more selective oxidant and is
- expected to react primarily with PAHs and other unsaturated compounds. PAHs constituted
- 380 <10% of the total precursor mass and the prevalence of functionalized organics was less than
- hydrocarbons by an order of magnitude. Yet, only slight difference was observed in the
- chemical composition of OA. This could be due to nucleation of unoxidized precursors being the
- dominant pathway of particle formation from emissions at 140°C as observed with HOA_{DC} in

- chamber tests. Despite similar chemical properties, the peak OA production of 0.8±0.4 mg OA
- min⁻¹ kg⁻¹ asphalt observed under NO₃ oxidation was slightly lower than 2.5±0.2 mg SOA min⁻¹
- kg⁻¹ asphalt from unseeded daytime oxidation tests as well as 4 ± 2.3 mg OA min⁻¹ kg⁻¹ asphalt
- 387 estimated in previous work.⁵

418

- While the gas-phase emissions at 140°C readily formed OA independent of photochemistry,
- precursor emissions at 60°C primarily included IVOCs⁵ that produced SOA mainly after
- undergoing photo-oxidation. Under daytime unseeded oxidation conditions, the resulting OA
- 391 (OFR-OA_{US60}) was highly aged with an O:C ratio of 0.7 and was primarily constituted by
- oxygenated compounds (62% C_xH_yO₁ and C_xH_yO_{>1} species). For reduced emissions at lower
- temperatures (e.g. 40-50°C), the f_{44} fraction in OA further increased by 35 80%, indicating
- further photooxidation for aerosol formation with reduced OHR_{ext} (Figure S15). We also
- observed that gas-phase oxidation products measured with PTR-ToF mainly constituted of small
- compounds with less than 8 carbon atoms in oxidation experiments with emissions at 140°C.
- However, the fraction of larger gaseous oxidation products (i.e., $C_{\#} > 8$) increased considerably
- in tests at 60°C, though their absolute abundance was greater at 140°C. This was possibly due to
- relatively lower OA mass loading in the reactor at 60°C, which reduced the condensational sink
- and gas-to-particle partitioning of gas-phase species as well as the OHR_{ext} thus increasing the
- 401 OH exposure of injected precursors (aged 1 2 equivalent days) (Figure S16).
- In addition to oxidized species, we also note minor contributions from precursor sulfur
- 403 containing organic compounds that were observed in the particle phase as sulfate (HRSO₄). Their
- signal enhanced linearly with total organics (HROrg) and were sensitive to UV exposure in OFR
- 405 tests (Section S2, Figure S17). Consistent with laboratory observations, a significant
- 406 enhancement in sulfate was also observed in Billerica during road paving in 2014 but not in 2020
- 407 (Figure S18), suggesting that high-temperature road paving could also make minor contributions
- 408 to ambient organosulfates at paving temperatures (Figures S17-18), but their absolute impact
- may depend on the asphalt material used in paving operations.
- The chamber and OFR tests showed that gas-phase emissions from asphalt can form OA in the
- atmosphere via both direct condensation and secondary oxidation pathways. Both these pathways
- were likely associated with enhancements in ambient OA downwind in Billerica during paving
- in 2014, yet asphalt-related OA can span a range of aging and chemical composition dependent
- on the type of emissions and oxidation conditions. While high-temperature (140°C) applications
- show a greater degree of HOA-like or less-aged aerosols, the OA formed via photo-oxidation
- spans lightly- to highly-aged OA under different emission and oxidation conditions.

3.3 Comparison of asphalt-related OA with source-specific and typical urban factors

- Here, we examine similarities in the chemical composition of asphalt-related OA from our
- 420 experiments and ambient data with OA from other sources and ambient factors previously

observed via PMF analysis. PMF often groups OA from sources that have similar chemical features. So, asphalt-related OA from our mix of laboratory and ambient measurements was compared to other urban sources and ambient factors to evaluate how its contributions might appear in comparison to different sources or urban areas in prior studies.

Comparisons to source-specific OA from previous experiments

First, we compare OA from our asphalt tests with prior laboratory or near-source observations of OA from a broad range of sources including fresh OA resulting from petrochemical, cooking, wood- and biomass-burning emissions. Asphalt-related OA could be difficult to isotopically differentiate from traditional combustion-based sources (e.g. vehicular exhaust) that are also derived from petroleum feedstocks. $^{70-72}$ However, its mass spectral features may vary depending on precursor and aging conditions. We obtained unit mass resolution spectra of these sources from the AMS spectral database (Table S2) 73,74 and compared them over a mass range of m/z 12 – 125, which constituted 90 – 95% of the total ion signal for different OA included in this analysis. The spectra of multiple sources within each category (e.g., different types of biomass-burning OA) were averaged prior to a category-wide comparison but are reported in Table S2. Lastly, each spectrum was normalized by the total ion signal in this range and compared via linear correlation and cosine angle similarity.

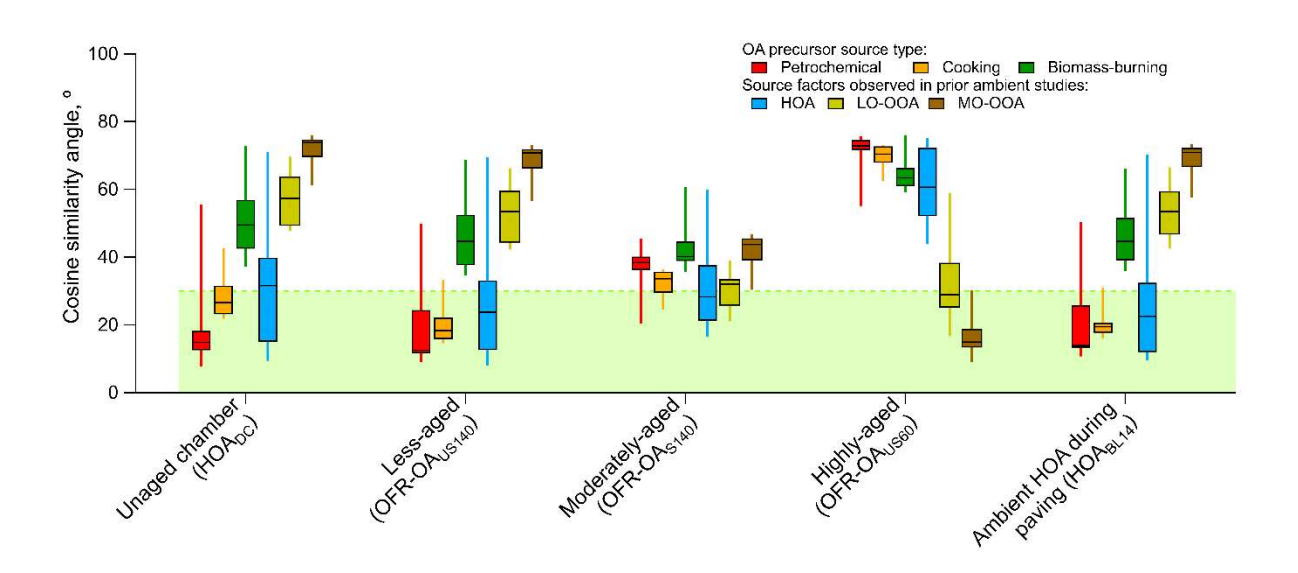


Figure 4. Comparison of OA produced from asphalt-related chamber and OFR experiments, as well as the HOA factor measured at the Aerodyne site during the road-paving event, with OA obtained from petrochemical, cooking and biomass burning emissions in prior laboratory experiments (see Table S2 for study descriptions), and with HOA, LO-OOA and MO-OOA factors from previous ambient studies (Table S3). The box plots show 0th, 25th, 50th, 75th, and 100th percentiles in cosine similarities and the green shaded region represents a cosine angle of ≤30° within which the spectra are considered comparable. Note: All experiments except the highly-aged (OFR) were performed with precursor emissions at paving temperature (140°C), while the highly-aged (OFR) involved precursor emissions at summertime road surface

448 temperatures (60°C). The terms less-, moderate- and highly-aged depend upon the degree of oxidation of the 449 OA formed in the OFR and are not to be confused with the equivalent aging during an experiment. In these comparisons, we primarily discuss asphalt-related OA at hot-mix paving temperature 450 (140°C) because at lower temperatures (60°C) after several days of photochemical aging, OFR-451 OA_{US60} was highly aged with f_{44} and f_{28} constituting >40% of the mass spectra and expectedly 452 did not correlate with any of the experiments without extensive oxidation in this study. On the 453 other hand, asphalt OA at 140°C was comparable to OA from petrochemical sources (Figure 4, 454 S19). For example, our chamber (HOADC, OALC) and unseeded OFR (OFR-OAUS140) tests 455 formed OA similar to combustion emissions from gasoline, diesel and plastics (cosine angle: 8° 456 457 -24° ; linear correlation coefficient, r > 0.85), with comparable m/z 44:43 and 55:57 ratios (Figures S19-20). Among all cases, the strongest similarities were observed between HOADC and 458 OA from gasoline emissions and lubricating oil (8°, r > 0.95) (Figure S21). HOA_{DC} was also 459 highly comparable to average OA from different diesel exhaust studies ($r > 0.9, 18^{\circ}$). Yet it 460 differed from diesel generator exhaust (r < 0.8 and 36°), which was more similar to aged OA_{LC} 461 462 and OFR-OA_{S140} (r > 0.9 and 21°). Outside gasoline and diesel sources, flaming coal-based OA showed comparable spectral features $(12^{\circ} - 34^{\circ})$, and similar m/z 44:43 and levoglucosan at m/z 463 (f_{60}) values. Asphalt-related OA was also sometimes similar to OA from meat-cooking 464 465 emissions ($16^{\circ} - 35^{\circ}$; r > 0.85) with comparable m/z 44:43 ratios (Figure S15), yet with m/z 466 55:57 and f_{60} values lower by factors of 2 and 10, respectively. 467 In contrast, asphalt OA was distinct from most wood/biomass burning-related OA (WBOA/BBOA) in our comparisons where mass spectra exhibited weak (r < 0.75) linear 468 correlations and large cosine angles (36° – 49°) (Figure 4, S19). WBOA and BBOA showed 469 470 strong levoglucosan signal (f_{60}) , which were absent in asphalt OA. It was also more oxygenated with an m/z 44:43 ratio of 0.25 - 1.4 versus 0.04 - 0.15 for asphalt and other petrochemical 471 472 sources (Figures S15, S20). 473

474

475

476

477

478

479

480 481

482

483

484

485

Comparisons to source apportioned OA factors from other ambient urban areas

The un-aged asphalt-related OA from our laboratory tests at application temperatures resembled prior urban HOA factors from AMS measurements in megacities in the U.S., Europe, and China (Figures 4, S22, Table S3)⁷⁴ as well as the ambient HOA factor observed in Billerica during paving in 2014 (Figure S23), which is consistent with prior observations by Faber et al.³⁵ who examined paving-adjacent enhancements closely resembling HOA (Figure S12). The application-related OA after 2.5 hours of aging in our chamber tests (OA_{LC}, Figure 3) was also comparable to ambient HOA factors from prior studies (cosine: 24°±14°) (Table S3, Figure S24), with expected variations in cosine similarity likely arising from slightly oxygenated aerosol mass fragments influencing ambient HOA factors. Interestingly, the unaged HOA from the chamber (HOA_{DC}) was broadly comparable (i.e., cosine <30°) to HOA from 40% of included ambient sites, with this fraction increasing to 80% for the slightly-aged OA_{LC}. Similarly, OA from both

seeded and unseeded OFR experiments (OFR-OA_{S140}, OFR-OA_{US140}) resembled HOA from 486 nearly 50% of the cities in prior work (Table S3). Yet, this similarity to urban HOA factors (and 487 other OOA factors below) does not suggest that the majority of HOA (or OOA) in urban areas is 488 asphalt-derived, but demonstrates the difficulty in distinguishing asphalt-related OA from other 489 490 petroleum-related sources. In the case of HOA, this is a reflection of asphalt's petroleum feedstocks and the inherent nature of PMF source factors representing a mix of sources with 491 similar molecular signatures. 492 Expectedly, increased aging reduced similarity to ambient HOA factors, but moderately and 493 494 highly aged OFR-OA also showed greater similarities with LO-OOA and MO-OOA ambient factors observed both in the 2014 near-paving ambient measurements and other urban studies 495 (Figure S22). For example in Figure 4, the highly oxidized OFR-OA_{US60} was expectedly 496 dissimilar to HOA from all sites (cosine similarity >30°) but was very similar to MO-OOA 497 498 obtained from all prior ambient studies considered here (Table S3). In summary, these comparisons with various major sources and ambient urban OA PMF source 499 factors show that distinguishing asphalt-related OA from the range of urban sources of direct OA 500 and reactive precursors is challenging. While fresh OA from hot-mix asphalt paving was 501 502 different from biomass-burning and meat cooking, it was statistically similar to OA from gasoline and diesel-related sources (Figure 4, S23) as well as HOA source factors in urban 503 studies. Furthermore, atmospheric aging of primary condensed OA or SOA formed from gas-504 phase precursors would contribute to the typically-observed LO-OOA and MO-OOA factors, 505

507 related emissions at summertime pavement temperatures, like the 60°C OFR studies here, the

resulting MO-OOA would be largely indistinguishable in ambient conditions (Figure 4). These 508

like those seen in the 2014 ambient measurements. In the case of highly aged OA from asphalt-

similarities across multiple atmospheric ages, coupled with fossil isotopic signature of asphalt-509 related emissions, 11 could potentially result in misattribution of asphalt-related OA to other

510

prominent urban sources in ambient measurements and top-down assessments of emissions 511 512

across asphalt's lifecycle. Further research is warranted to develop methods (e.g. identification of

marker species, isolating volatility-dependent contributions) to constrain the impact of asphalt-513

related emissions on urban OA. 514

515

516

506

Acknowledgements

- We acknowledge funding from U.S. NSF (grants: AGS-2131368 (Aerodyne); CBET-2011362, 517
- AGS-2131084 (Yale University); and CBET-1907446, AGS-1848324 (Carnegie Mellon 518
- University)). The 2014 ambient data in Billerica, MA was collected with support from the U.S. 519
- 520 Department of Energy (DESC0004698). We also acknowledge the U.S. EPA; this publication
- 521 was developed under Assistance Agreements No. RD835871 and 83587301 awarded by the U.S.
- Environmental Protection Agency to Yale University and Carnegie Mellon University, 522
- respectively. It has not been formally reviewed by EPA. The views expressed in this document 523

- are solely those of the authors and do not necessarily reflect those of the Agency. EPA does not
- endorse any products or commercial services mentioned in this publication. We also thank Yale
- Facilities for helping acquire the PG 64-22 road asphalt during a road resurfacing event in New
- Haven, CT; and Rishabh Shah (formerly at CIRES) for helpful discussions on ToF-AMS
- 528 analysis.

530

References

- Hass-Mitchell, T. *et al.* Increasing Contributions of Temperature-Dependent Oxygenated Organic Aerosol to Summertime Particulate Matter in New York City. *ACS ES&T Air* 1, 113–128 (2024).
- 534 2. Jimenez, J. L. *et al.* Evolution of organic aerosols in the atmosphere. *Science* **326**, 1525–1529 (2009).
- 536 3. Kroll, J. H. & Seinfeld, J. H. Chemistry of secondary organic aerosol: Formation and evolution of low-volatility organics in the atmosphere. *Atmos. Environ.* **42**, 3593–3624 (2008).
- Zhao, Y. et al. Reducing secondary organic aerosol formation from gasoline vehicle
 exhaust. Proc. Natl. Acad. Sci. U. S. A. 114, 6984–6989 (2017).
- 5. Khare, P. *et al.* Asphalt-related emissions are a major missing nontraditional source of secondary organic aerosol precursors. *Sci. Adv.* **6**, eabb9785 (2020).
- 6. Gentner, D. R. *et al.* Emissions of terpenoids, benzenoids, and other biogenic gas-phase organic compounds from agricultural crops and their potential implications for air quality.

 Atmos. Chem. Phys. Discuss. 13, 28343–28393 (2013).
- He, M. *et al.* Total organic carbon measurements reveal major gaps in petrochemical emissions reporting. *Science* **383**, 426–432 (2024).
- Pennington, E. A. *et al.* Modeling secondary organic aerosol formation from volatile chemical products. *Atmos. Chem. Phys.* **21**, 18247–18261 (2021).
- 550 9. Kroll, J. H. & Seinfeld, J. H. Chemistry of secondary organic aerosol: Formation and evolution of low-volatility organics in the atmosphere. *Atmos. Environ.* **42**, 3593–3624 (2008).
- 553 10. Guenther, A. Biological and Chemical Diversity of Biogenic Volatile Organic Emissions into the Atmosphere. *ISRN Atmos. Sci.* **2013**, 1–27 (2013).
- 555 11. Khare, P. & Gentner, D. R. Considering the future of anthropogenic gas-phase organic 556 compound emissions and the increasing influence of non-combustion sources on urban air 557 quality. *Atmos. Chem. Phys* **18**, 5391–5413 (2018).
- 558 12. Mcdonald, B. C. *et al.* Volatile chemical products emerging as largest petrochemical source of urban organic emissions. *Science* (80-.). **359**, 760–764 (2018).
- 560 13. Gkatzelis, G. I. et al. Observations Confirm that Volatile Chemical Products Are a Major

- Source of Petrochemical Emissions in U.S. Cities. *Environ. Sci. Technol.* **55**, 4332–4343 (2021).
- 563 14. Seltzer, K. M. *et al.* Anthropogenic secondary organic aerosol and ozone production from asphalt-related emissions. *Environ. Sci. Atmos.* **3**, 1221–1230 (2023).
- Wang, F. *et al.* Characteristics of VOCs generated during production and construction of an asphalt pavement. *Transp. Res. Part D Transp. Environ.* **87**, 102517 (2020).
- 567 16. Cui, P., Wu, S., Xiao, Y. & Zhang, H. Study on the deteriorations of bituminous binder 568 resulted from volatile organic compounds emissions. *Constr. Build. Mater.* **68**, 644–649 569 (2014).
- Movilla-Quesada, D. *et al.* Analysis of Greenhouse Gas Emissions and the Environmental
 Impact of the Production of Asphalt Mixes Modified with Recycled Materials. *Sustain.* 2021, 13, 8081 (2021).
- 573 18. Farshidi, F. *et al.* Direct Measurements of Volatile and Semivolatile Organic Compounds 574 from Hot- and Warm-Mix Asphalt. *Transp. Res. Rec.* **2207**, 1–10 (2011).
- 575 19. Kriech, D. M., Crawford, A. C., Smith, L. A., Osborn, L. V. & Kriech, A. J. Characterizing asphalt emissions under in-service conditions. *Atmos. Environ. X* 16, 100196 (2022).
- 578 20. Boczkaj, G., Przyjazny, A. & Kami Ski, M. Characteristics of volatile organic compounds emission profiles from hot road bitumens. *Chemosphere* **107**, 23–30 (2014).
- 580 21. Kitto, A. M. *et al.* Emissions of Volatile and Semi-Volatile Organic Compounds and Particulate Matter from Hot Asphalts. *Environ. Technol.* **18**, 121–138 (1997).
- Mo, S., Wang, Y., Xiong, F. & Ai, C. Effects of asphalt source and mixing temperature on the generated asphalt fumes. *J. Hazard. Mater.* **371**, 342–351 (2019).
- Jullien, A. et al. Airborne Emissions Assessment of Hot Asphalt Mixing. Road Mater.
 Pavement Des. 11, 149–169 (2011).
- Martin, H., Kerstin, Z. & Joachim, M. Reduced emissions of warm mix asphalt during construction. *Road Mater. Pavement Des.* **20**, S568–S577 (2019).
- 588 25. Gundla, A. & Shane Underwood, B. Molecular weight distribution of asphalt binders from Laser Desorption Mass Spectroscopy (LDMS) technique and its relationship to linear viscoelastic relaxation spectra. *Fuel* **262**, 116444 (2020).
- 591 26. Niles, S. F., Chacón-Patiño, M. L., Putnam, S. P., Rodgers, R. P. & Marshall, A. G.
- Characterization of an Asphalt Binder and Photoproducts by Fourier Transform Ion Cyclotron Resonance Mass Spectrometry Reveals Abundant Water-Soluble
- 594 Hydrocarbons. *Environ. Sci. Technol.* **54**, 8830–8836 (2020).
- Tyler, S. C., Lowe, D. C., Dlugokencky, E., Zimmerman, P. R. & Cicerone, R. J. Methane and carbon monoxide emissions from asphalt pavement: Measurements and estimates of their importance to global budgets. *J. Geophys. Res.* **95**, 14007 (1990).
- 598 28. Lasne, J. et al. NOx emissions by real-world fresh and old asphalt mixtures: Impact of

- temperature, relative humidity, and UV-irradiation. *Urban Clim.* **49**, 101457 (2023).
- Lasne, J. *et al.* VOC emissions by fresh and old asphalt pavements at service temperatures: impacts on urban air quality. *Environ. Sci. Atmos.* 3, 1601-1619 (2023).
- doi:10.1039/D3EA00034F
- Humes, M. B. *et al.* Primary and Secondary Organic Aerosol Formation from Asphalt Pavements. *Environ. Sci. Technol.* **57**, 20034–20042 (2023).
- Glattke, T. J., Chacon-Patino, M. L., Marshall, A. G. & Rodgers, R. P. Maltene and Asphaltene Contributions to the Formation of Water-Soluble Emerging Contaminants from Photooxidation of Paving Materials. *Energy and Fuels* **36**, 13060–13072 (2022).
- Chong, D., Wang, Y., Zhao, K., Wang, D. & Oeser, M. Asphalt Fume Exposures by
 Pavement Construction Workers: Current Status and Project Cases. *J. Constr. Eng. Manag.* 144, 05018002 (2018).
- 33. Xu, Y., Lindh, C. H., Jönsson, B. A. G., Broberg, K. & Albin, M. Occupational exposure to asphalt mixture during road paving is related to increased mitochondria DNA copy number: A cross-sectional study. *Environ. Heal. A Glob. Access Sci. Source* 17, 1–10 (2018).
- 615 34. McClean, M. D. *et al.* Inhalation and Dermal Exposure among Asphalt Paving Workers. *Ann. Occup. Hyg.* **48**, 663–671 (2004).
- Faber, P., Drewnick, F. & Borrmann, S. Aerosol particle and trace gas emissions from earthworks, road construction, and asphalt paving in Germany: Emission factors and influence on local air quality. *Atmos. Environ.* **122**, 662–671 (2015).
- Zhang, X. *et al.* Highly Oxygenated Multifunctional Compounds in α-Pinene Secondary
 Organic Aerosol. *Environ. Sci. Technol.* 51, 5932–5940 (2017).
- Zhang, Y. et al. Effect of the Aerosol-Phase State on Secondary Organic Aerosol
 Formation from the Reactive Uptake of Isoprene-Derived Epoxydiols (IEPOX). Environ.
 Sci. Technol. Lett. 5, 167–174 (2018).
- 38. Nah, T., Sanchez, J., Boyd, C. M. & Ng, N. L. Photochemical Aging of α-pinene and β-pinene Secondary Organic Aerosol formed from Nitrate Radical Oxidation. *Environ. Sci. Technol.* 50, 222–231 (2016).
- Lambe, A. T. *et al.* Relationship between oxidation level and optical properties of secondary organic aerosol. *Environ. Sci. Technol.* **47**, 6349–6357 (2013).
- Chowdhury, P. H. *et al.* Exposure of Lung Epithelial Cells to Photochemically Aged
 Secondary Organic Aerosol Shows Increased Toxic Effects. *Environ. Sci. Technol. Lett.* 5,
 424–430 (2018).
- 633 41. Chowdhury, P. H. *et al.* Connecting the Oxidative Potential of Secondary Organic 634 Aerosols with Reactive Oxygen Species in Exposed Lung Cells. *Environ. Sci. Technol.* 635 **53**, 13949–13958 (2019).
- 636 42. Li, R. et al. Laboratory studies on secondary organic aerosol formation from crude oil

- 637 vapors. Environ. Sci. Technol. 47, 12566–12574 (2013).
- Bahreini, R. *et al.* Mass spectral analysis of organic aerosol formed downwind of the deepwater horizon oil spill: Field studies and laboratory confirmations. *Environ. Sci. Technol.* 46, 8025–8034 (2012).
- Shah, R. U. *et al.* Urban Oxidation Flow Reactor Measurements Reveal Significant
 Secondary Organic Aerosol Contributions from Volatile Emissions of Emerging
 Importance. *Environ. Sci. Technol.* 54, 714–725 (2020).
- 644 45. Palm, B. B. *et al.* Secondary organic aerosol formation from ambient air in an oxidation flow reactor in central Amazonia. *Atmos. Chem. Phys.* **18**, 467–493 (2018).
- Kang, E. *et al.* Photochemical aging of aerosol particles in different air masses arriving at Baengnyeong Island, Korea. *Atmos. Chem. Phys.* **18**, 6661–6677 (2018).
- 648 47. Ahlberg, E. *et al.* No Particle Mass Enhancement from Induced Atmospheric Ageing at a Rural Site in Northern Europe. *Atmosphere (Basel).* **10**, 408 (2019).
- Janechek, N. J. *et al.* Physical properties of secondary photochemical aerosol from OH oxidation of a cyclic siloxane. *Atmos. Chem. Phys.* **19**, 1649–1664 (2019).
- Liu, P. S. K. *et al.* Transmission Efficiency of an Aerodynamic Focusing Lens System:
 Comparison of Model Calculations and Laboratory Measurements for the Aerodyne
 Aerosol Mass Spectrometer. *Aerosol Sci. Technol.* 41, 721–733 (2007).
- 50. DeCarlo, P. F. *et al.* Field-deployable, high-resolution, time-of-flight aerosol mass spectrometer. *Anal. Chem.* **78**, 8281–8289 (2006).
- 51. Budisulistiorini, S. H. *et al.* Intercomparison of an Aerosol Chemical Speciation Monitor
 (ACSM) with ambient fine aerosol measurements in downtown Atlanta, Georgia. *Atmos. Meas. Tech.* 7, 1929–1941 (2014).
- Middlebrook, A. M., Bahreini, R., Jimenez, J. L. & Canagaratna, M. R. Evaluation of
 Composition-Dependent Collection Efficiencies for the Aerodyne Aerosol Mass
 Spectrometer using Field Data. Aerosol Sci. Technol. 46, 258–271 (2012).
- 663 53. Atkinson, R. Kinetics and Mechanisms of the Gas-Phase Reactions of the NO3 Radical with Organic Compounds. *J. Phys. Chem. Ref. Data* **20**, 459–507 (1991).
- Lambe, A. *et al.* Controlled nitric oxide production via O(1D)+N2O reactions for use in oxidation flow reactor studies. *Atmos. Meas. Tech. Discuss.* 1–20 (2017).
 doi:10.5194/amt-2016-394
- Peng, Z. et al. Model Evaluation of New Techniques for Maintaining High-NO
 Conditions in Oxidation Flow Reactors for the Study of OH-Initiated Atmospheric
 Chemistry. ACS Earth Sp. Chem. 2, 72–86 (2018).
- 671 56. Rowe, J. P., Lambe, A. T. & Brune, W. H. Technical Note: Effect of varying the λ = 185
 672 and 254nm photon flux ratio on radical generation in oxidation flow reactors. *Atmos.* 673 *Chem. Phys.* 20, 13417–13424 (2020).
- 674 57. Mao, J. et al. Airborne measurement of OH reactivity during INTEX-B. Atmos. Chem.

- 675 *Phys.* **9**, 163–173 (2009).
- 58. Lambe, A. T. *et al.* Nitrate radical generation via continuous generation of dinitrogen pentoxide in a laminar flow reactor coupled to an oxidation flow reactor. *Atmos. Meas. Tech.* **13**, 2397–2411 (2020).
- 59. Chemical Speciation Network Parameters Reported to the Air Quality System (AQS) |
 US EPA. Available at: https://www.epa.gov/amtic/chemical-speciation-network-parameters-reported-air-quality-system-aqs. (Accessed: 28th April 2023)
- 682 60. Kang, C. M., Koutrakis, P. & Suh, H. H. Hourly Measurements of Fine Particulate Sulfate 683 and Carbon Aerosols at the Harvard–U.S. Environmental Protection Agency Supersite in 684 Boston. *J. Air Waste Manage. Assoc.* **60**, 1327 (2010).
- 685 61. Schroder, J. C. *et al.* Sources and Secondary Production of Organic Aerosols in the 686 Northeastern United States during WINTER. *J. Geophys. Res. Atmos.* **123**, 7771–7796 687 (2018).
- 688 62. Zhang, J. *et al.* The Response of Summertime Organic Aerosol Composition to Emission Controls in the Northeastern United States. *J. Geophys. Res. Atmos.* **127**, e2022JD037056 (2022).
- 63. Aiken, A. C. *et al.* O/C and OM/OC ratios of primary, secondary, and ambient organic aerosols with high-resolution time-of-flight aerosol mass spectrometry. *Environ. Sci. Technol.* **42**, 4478–4485 (2008).
- 694 64. Zhang, Q., Worsnop, D. R., Canagaratna, M. R. & Jimenez, J. L. Hydrocarbon-like and oxygenated organic aerosols in Pittsburgh: insights into sources and processes of organic aerosols. *Atmos. Chem. Phys.* **5**, 3289–3311 (2005).
- 65. Canagaratna, M. R. *et al.* Chase Studies of Particulate Emissions from in-use New York City Vehicles. *Aerosol Sci. Technol.* **38**, 555–573 (2004).
- 699 66. Arey, J. *et al.* Dicarbonyl products of the OH radical-initiated reaction of a series of aromatic hydrocarbons. *Environ. Sci. Technol.* **43**, 683–689 (2009).
- Zaytsev, A. et al. Mechanistic study of the formation of ring-retaining and ring-opening products from the oxidation of aromatic compounds under urban atmospheric conditions.
 Atmos. Chem. Phys. 19, 15117–15129 (2019).
- 704 68. Zhang, X. *et al.* Influence of vapor wall loss in laboratory chambers on yields of secondary organic aerosol. *Proc. Natl. Acad. Sci. U. S. A.* **111**, 5802–5807 (2014).
- Ma, P. K. *et al.* Evaluating the impact of new observational constraints on P-S/IVOC
 emissions, multi-generation oxidation, and chamber wall losses on SOA modeling for Los
 Angeles, CA. *Atmos. Chem. Phys* 17, 9237–9259 (2017).
- 70. Dai, S. *et al.* Chemical and stable carbon isotopic composition of PM2.5 from on-road vehicle emissions in the PRD region and implications for vehicle emission control policy. *Atmos. Chem. Phys.* **15**, 3097–3108 (2015).
- 71. Wu, X. et al. Characterization and source apportionment of carbonaceous PM2.5 particles

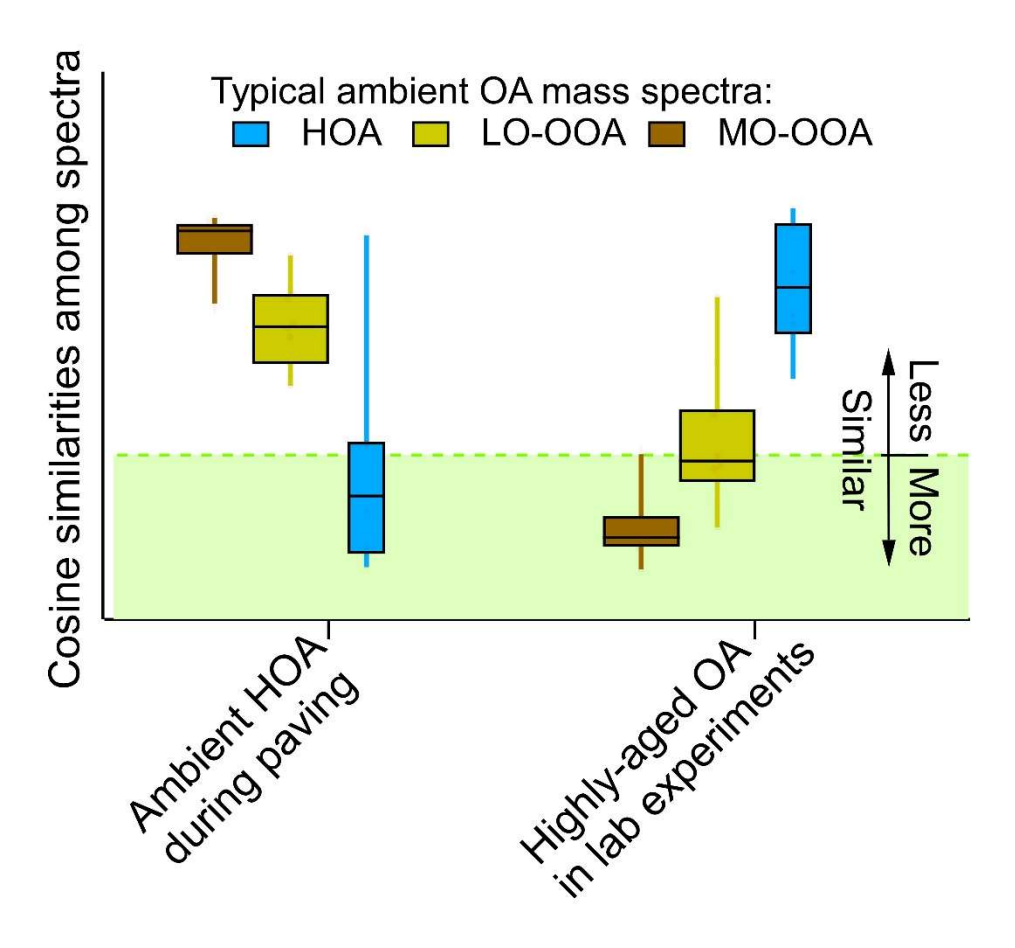
713 in China - A review. *Atmospheric Environment* **189**, 187–212 (2018).

722

- 72. Cao, F. *et al.* New insights into the sources and formation of carbonaceous aerosols in China: Potential applications of dual-carbon isotopes. *National Science Review* **4**, 804–806 (2017).
- 717 73. Ulbrich, I. M., Canagaratna, M. R., Zhang, Q., Worsnop, D. R. & Jimenez, J. L.

 718 Interpretation of organic components from Positive Matrix Factorization of aerosol mass

 719 spectrometric data. *Atmos. Chem. Phys.* **9**, 2891–2918 (2009).
- 74. Ulbrich, I.M., Handschy, A., Lechner, M., and Jimenez, J. L. AMS Spectral Database.
 Available at: http://cires.colorado.edu/jimenez-group/AMSsd/. (Accessed: 6th June 2023)



725 <u>TOC art figure</u>

Contents of the supporting information file

Overview of the Billerica sampling site location and wind data; supplemental ambient observations, positive matrix factorization results, and their interpretation; additional details on laboratory oxidation experiments and associated results; supplemental comparisons with organic aerosol mass spectra from previous ambient and chamber experiments.